iScience

CellPress

Article

Detection of Extracellular Vesicle RNA Using Molecular Beacons

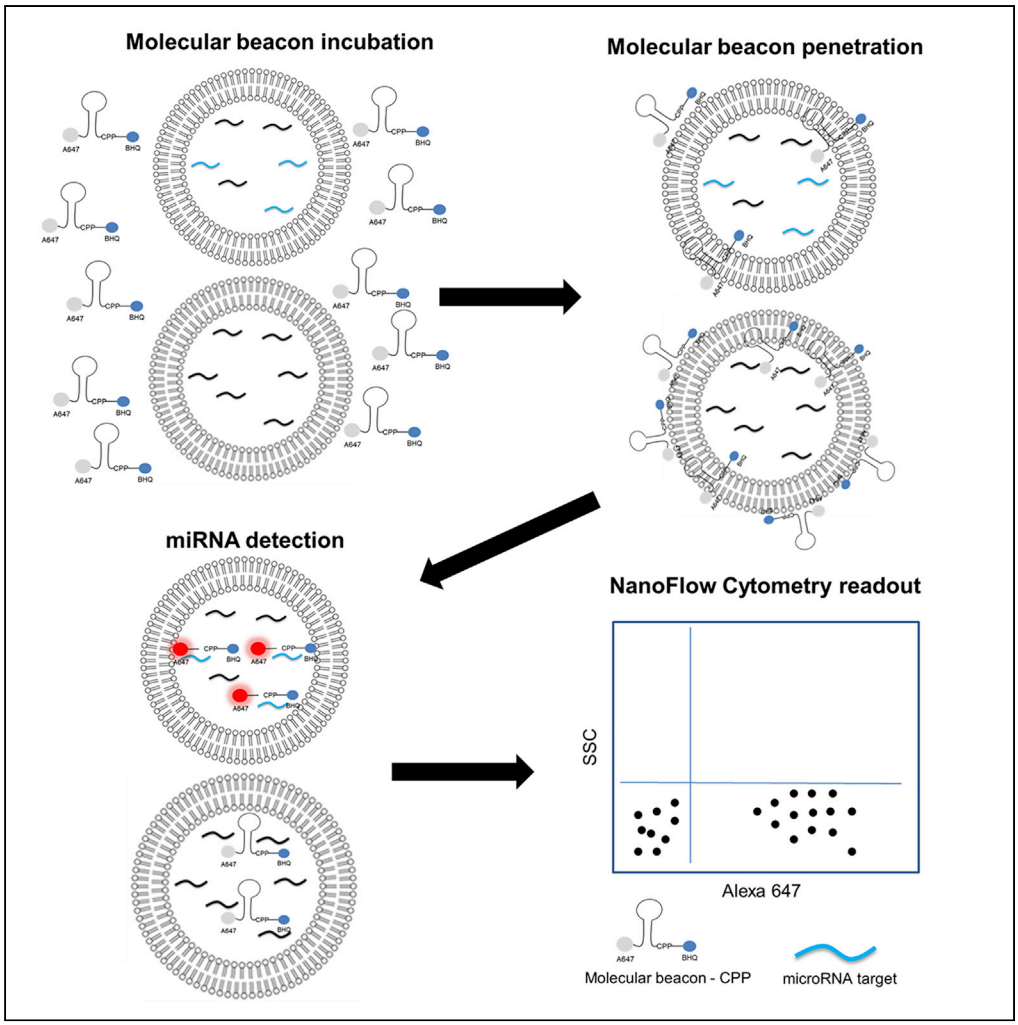

Getulio Pereira de Oliveira, Jr., Eric Zigon, Gaenna Rogers, ..., John Tigges, Sanjay Tyagi, Ionita Calin Ghiran

ighiran@bidmc.harvard.edu

HIGHLIGHTS

RBC and RBC-EVs contain unequal amount of RNA

Efficient detection of miRNA *in vitro* by MBs using nano-flow cytometry

CPPs effectively deliver cargo to cells and extracellular vesicles

MB-CPP can be used to detect cell-specific EV miRNAs

Oliveira et al., iScience *23*, 100782
January 24, 2020
https://doi.org/10.1016/j.isci.2019.100782

iScience

CellPress

Article

Detection of Extracellular Vesicle RNA Using Molecular Beacons

Getulio Pereira de Oliveira, Jr.,[1] Eric Zigon,[2] Gaenna Rogers,[2] Danny Davodian,[1,3] Shulin Lu,[1] Tijana Jovanovic-Talisman,[4] Jennifer Jones,[5] John Tigges,[2] Sanjay Tyagi,[6,7] and Ionita Calin Ghiran[1,7,8,*]

SUMMARY

Extracellular vesicles (EVs) have recently emerged as intercellular conveyors of biological information and disease biomarkers. Identification and characterization of RNA species in single EVs are currently challenging. Molecular beacons (MBs) represent an attractive means for detecting specific RNA molecules. Coupling the MBs to cell-penetrating peptides (CPPs) provides a fast, effective, and membrane-type agnostic means to deliver MBs across the plasma membrane and into the cytosol. Here, we generated RBCs-derived EVs by complement activation and tested the ability of MBs coupled with CPP to detect miRNAs from RBC-EVs. Our results showed that RBC and RBC-EVs miRNA-451a can be detected using MB-CPP, and the respective fluorescence levels can be measured by nano-flow cytometry. MB-based detection of RNA via nano-flow cytometry creates a powerful new analytical framework in which a simple addition of a reagent allows profiling of specific RNA species present within certain EV subsets.

INTRODUCTION

A novel paradigm in paracrine signaling has recently emerged based on the findings identifying extracellular vesicles (EVs) as multifaceted, intercellular conveyors of biological information (Tkach and Thery, 2016; Thery, 2015). EVs and their cargo have been shown to regulate gene expression and alter cell function in various cell types (Kreimer et al., 2015; Mantel et al., 2013). Isolation and molecular profiling of subsets of EVs (i.e., RNAs, proteins, lipids, metabolites) are critical for understanding the biogenesis of EVs and their potential utility as biomarkers. Simultaneous, multiparametric characterization of external protein and internal RNA components of single EVs is currently challenging owing to the limitations of currently available EV analysis assays. These require bulk analyses, thus limiting the detection of low abundant EV components and detection of EV DNA/RNA/proteins, and involves time-consuming (RNA-seq, dd/q-RT-PCR, southern/northern/western blot), as well as expensive (-omics) analyses.

Using the EV RNA cargo as an indicator of tissue origin or disease marker relies on identifying and quantifying the expression level of various RNA species from isolated EVs. When analyzing EV populations for low copy number of RNAs, it is easy to underappreciate rare signal, which may contain critical information about incipient processes in the host, as the information obtained represents an average and does not account for EV heterogeneity.

Molecular beacons (MBs) are hairpin-shaped oligonucleotides that contain a complementary sequence to a specific RNA or ssDNA molecule, a fluorochrome, and a quencher (Giesendorf et al., 1998; Tyagi and Kramer, 1996). Upon binding to target, MB undergoes a conformation change that separates the quencher from the fluorochrome, thus allowing the probe to fluoresce upon excitation. We have shown that the binding between the DNA/RNA target and MB is highly specific, with even one pair mismatch anywhere on the sequence preventing the opening of the stem and thus keeping the MB non-fluorescent (Bonnet et al., 1999; Marras et al., 1999; Tyagi et al., 1998). Most if not all extracellular and intracellular RNA species are bound to various RNA-binding proteins, interactions that could potentially interfere with the MB-based detection approach. Since the binding affinities of oligonucleotide probes to their targets are at least an order of magnitude higher than the binding affinities of RNA-binding proteins to their targets, MBs are successfully able to bind to mRNAs in living cells by displacing the bound proteins (Bratu et al., 2003; Chen et al., 2017b; Vargas et al., 2005).

Cell-penetrating peptides (CPPs) are short peptide sequences, rich in lysine or arginine, that have the ability to cross biological membranes through either passive or active processes. Based on their overall charge,

[1]Division of Allergy and Inflammation, Department of Medicine, Beth Israel Deaconess Medical Center, Harvard Medical School, Boston, MA, USA

[2]Nano Flow Core Facility, Beth Israel Deaconess Medical Center, Harvard Medical School, Boston, MA, USA

[3]Centre for Prehospital and Emergency Research, Department of Clinical Medicine, Aalborg University, Aalborg, Denmark

[4]Department of Molecular Medicine, Beckman Research Institute, City of Hope Comprehensive Cancer Center, Duarte, CA, USA

[5]Laboratory of Pathology Center for Cancer Research, National Cancer Institute, Bethesda, MD, USA

[6]Public Health Research Institute, New Jersey Medical School, Rutgers, The State University of New Jersey, Newark, NJ, USA

[7]These authors contributed equally

[8]Lead Contact

*Correspondence: ighiran@bidmc.harvard.edu

https://doi.org/10.1016/j.isci.2019.100782

CPPs belong to three distinct classes: cationic, amphipathic, and hydrophobic, each of which use a distinct mechanism for membrane fusion and internalization, although the precise molecular mechanisms are still poorly understood (Vives et al., 2003). As CPPs can be coupled to a wide range of biological compounds, they represent an attractive delivery vehicle perfectly suited to bridge the gap between specific RNA detection, imaging- and flow-friendly readouts, and simplicity of use. CPPs coupled to MBs have been used for tracking mRNA in living cells successfully before (Nitin et al., 2004).

We herein describe a novel method for interrogating the RNA content of circulating EVs, which combines the sensitivity and specificity of MBs to provide specific RNA information with the high throughput of nano-flow cytometry (nFC) for detection of specific RNA molecules in subsets of EVs. Our results show that interrogating cells and EVs with MBs coupled to CPPs provides fast and reliable results, which are fully consistent with more sophisticated, and time consuming, RNA detection methods such as q-RT-PCR.

RESULTS

Extracellular Vesicles Contain Unequal Amount of RNA

Imaging and tracking small RNA molecules in cells, without the use of involved methods such as microinjection of labeled RNA molecules or RNA *in situ* hybridization, is complicated by the lack of exclusive RNA dyes, the presence of large amounts DNA in nucleus and mitochondria (~13 kb), and the existence of significant levels of *m*, *r*, and *t* RNAs in cytosol. Red blood cells, by lacking organelles, DNA, and mRNA molecules, offer a significant advantage for studying EV biogenesis (originating from plasma membrane, i.e., microparticles) and RNA loading into EVs. We and others have shown that circulating RBCs contain few species and copies of small non-coding RNAs (sRNAs) relevant in host pathogen interaction (LaMonte et al., 2012; Mantel et al., 2016), and reviewed by Walzer et al. (Walzer and Chi, 2017). Using Syto9, a membrane-permeable RNA selective dye (Figure 1A, left panel, arrows), the RNA content of RBCs can be successfully labeled and tracked as it is packaged into EVs. Importantly, the RNA content of circulating RBCs decreases with the age of the cells, with newly released RBCs from bone marrow containing the largest amount of sRNAs (Figure 1A, middle panel, reticulocytes), whereas the older, smaller RBCs having virtually non-detectable sRNAs by fluorescence microscopy (Figure 1A, right panel, old RBC). A similar trend was observed when new, intermediate, and old RBCs were isolated from three independent donors using Percoll gradient and total RNA was quantified by fluorometry (Qubit, Thermo Fisher) (Figure 1B). Next, we took advantage of the uncluttered RNA landscape of human RBCs to quantify the range of sRNAs present in complement-generated EVs following our validated protocol (Kuo et al., 2017). The efficacy of complement-mediated EV generation was verified by transmission electron microscopy (Figure 1C), resistive pulse sensing (qNano, Izon) (Figure 1D), and nano-flow cytometry (Figure 1E, gate "EVs"). Next, the total RNA in RBC-EVs was labeled using Syto9 as show above. Our results show that even if the EVs were generated from the same cell type (RBCs) using the same method (complement activation, Figure 1F), their RNA content was not uniformly distributed among EVs (Figure 1G). Although virtually all EVs contain some amounts of sRNAs (Figure 1G, see the sub-log, unimodal shift of the main EV population), a subpopulation of EVs contained larger (over a log fluorescence difference) amounts, and presumably different types or sequences of sRNA (Figure 1G, arrow). Therefore, we investigated the effectiveness of MBs to label only EVs containing specific miRNA sequence, thus bypassing the need for EV isolation and purification as well as RNA-seq or qPCR.

Detection of miRNA by MBs Using Fluorometry and Nano-Flow Cytometry

Current detection of specific miRNAs species is performed using RNA-seq or targeted qPCR-based approaches, which implies the use of involved and time-consuming procedures. MBs offer a one-step direct approach based on direct hybridization of the probe to the target nucleic acid sequence. We tested the ability of bead-attached MBs and CPP-coupled MB to identify the presence of specific miRNAs in buffer by incubating increasing concentrations of target or scrambled control miRNAs with complementary MBs immobilized on 10-μm sepharose beads (Figures S1 and S2). Our results, consistent with previous reports (Mhlanga and Tyagi, 2006; Nitin et al., 2004; Tyagi and Kramer, 1996), show a direct relationship between the concentration of the target miRNAs and fluorescence of the MBs attached to streptavidin-sepharose beads. The lowest concentration of miRNAs immobilized on beads that generated a significant fluorescence signal (MFI 6.22) over the control scramble miRNAs (MFI 4.01) was 5 nM. Each streptavidin-sepharose bead would immobilize between 5,000 and 12,000 MBs, explaining the large fluorescence shift observed with higher concentrations of miRNAs. However, it is unlikely that such large numbers of the same miRNA species are present in any given EV or EV subpopulation. Thus, we tested the ability of our approach

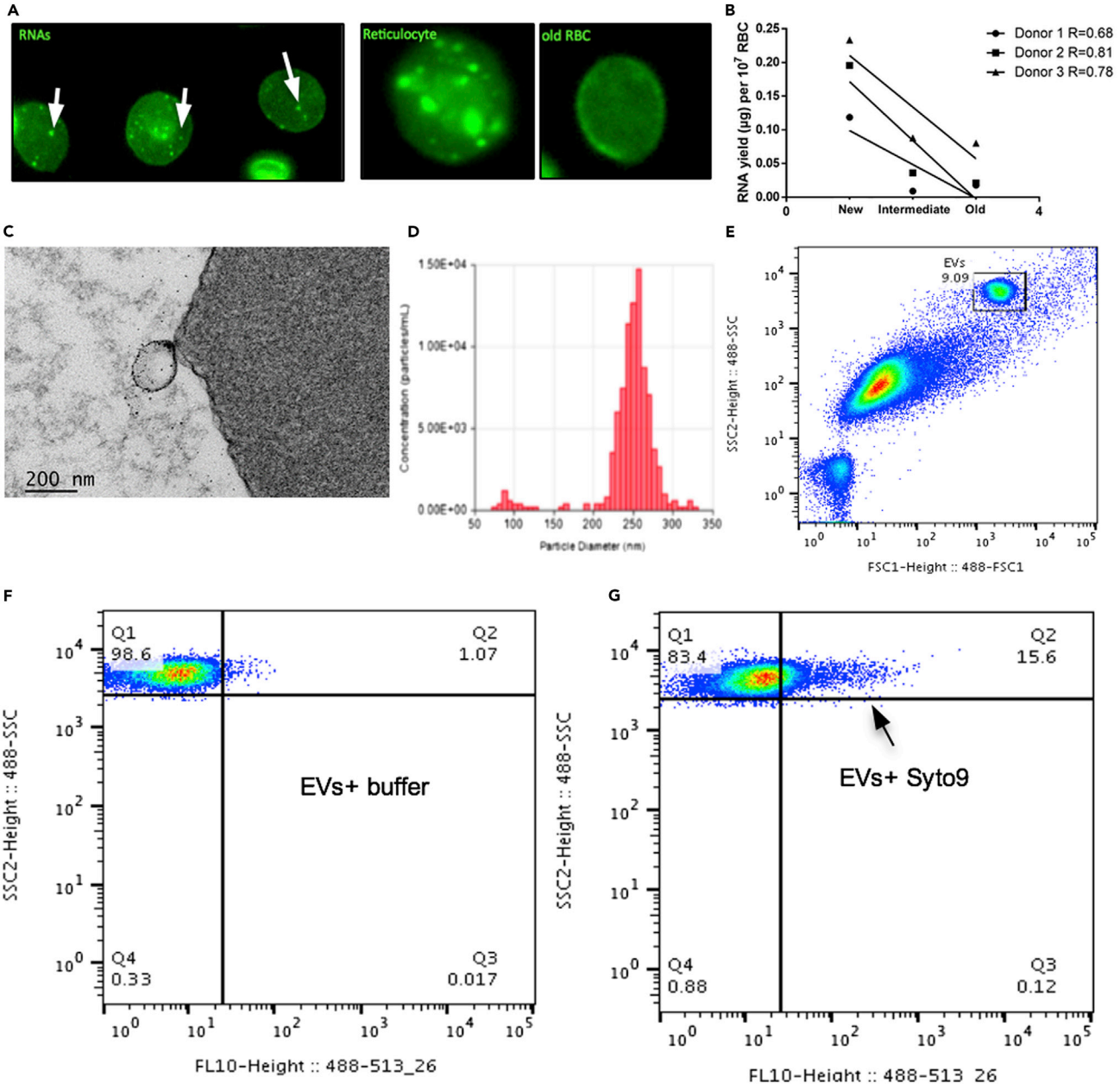

Figure 1. EVs from the Same Cell Type Have Uneven RNA Loading

(A) Human RBC labeled for sRNA showing circulating age-related loss of cell sRNA (top row).

(B) Correlation plot of the total RNA content of old, intermediate, and new RBCs from three independent donors.

(C) Electron micrograph of an EV budding from RBC plasma membrane showing lack of or minimal amounts of hemoglobin content compared with the concentration of cytoplasmic hemoglobin of the parent cell.

(D) RBC-EVs diameters were measured using resistive pulse sensing (qNano).

(E–G) (E). Nano-flow cytometry of RBC-derived EVs in the presence of buffer (F) or 5 nM Syto9 (G), showing uneven RNA staining in EV population.

to detect physiologically relevant concentrations of miRNA using platelets and RBCs, two of the most abundant cell types in the blood and major contributors to circulating EVs.

Membrane-Penetrating Peptides Effectively Deliver Cargo to Cells and Extracellular Vesicles

We started by testing the efficacy of fluorescently labeled cell-perpetrating peptides, based on TAT sequence (CPP-FAM) to cross the plasma membrane and label circulating cells. We incubated freshly

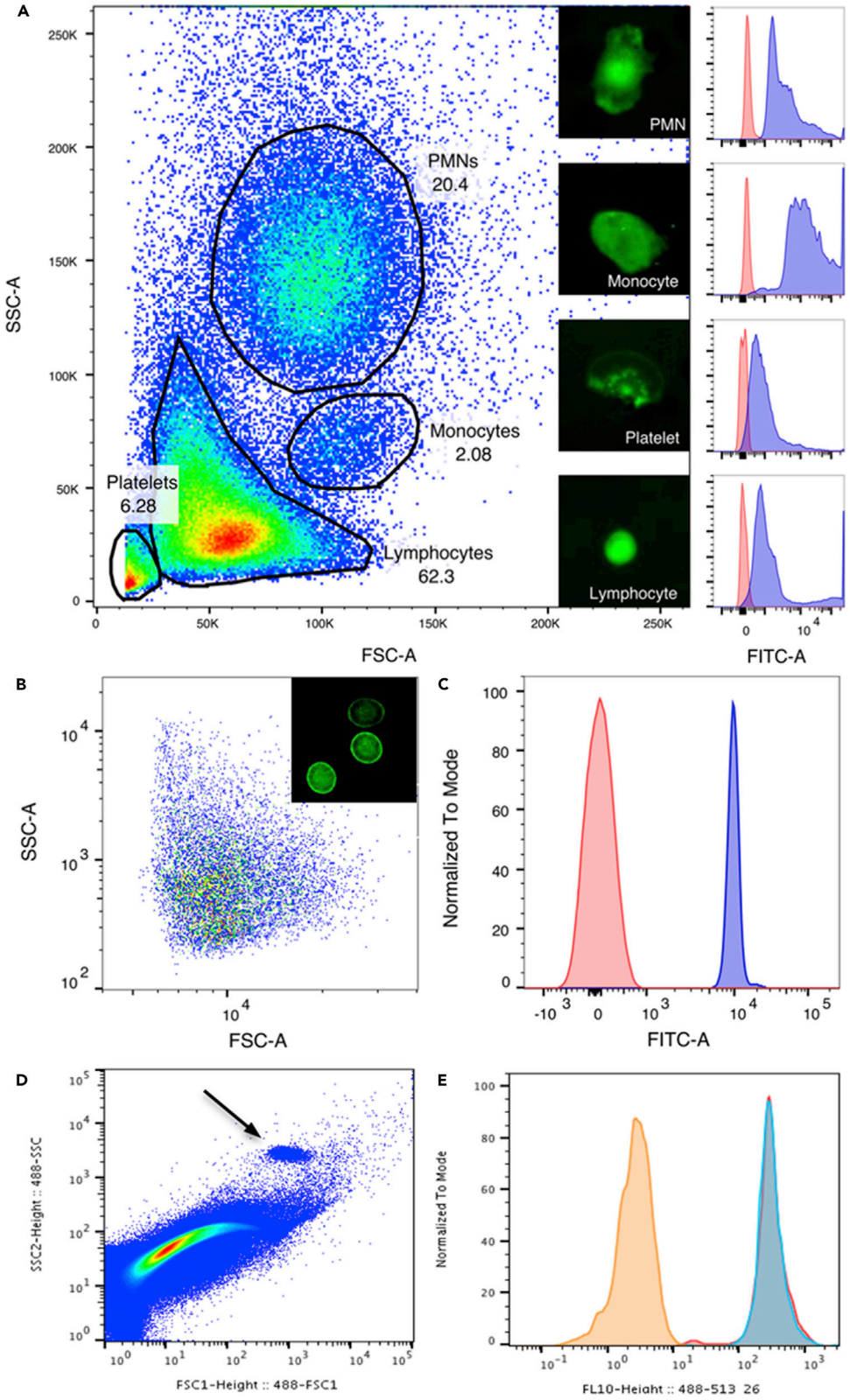
A
SSC-A
FSC-A
FITC-A
PMNs
20.4
Monocytes
2.08
Platelets
6.28
Lymphocytes
62.3
PMN
Monocyte
Platelet
Lymphocyte
B
SSC-A
FSC-A
C
Normalized To Mode
FITC-A
D
SSC2-Height :: 488-SSC
FSC1-Height :: 488-FSC1
E
Normalized To Mode
FL10-Height :: 488-513 26

Figure 2. CPPs Effectively Deliver Cargo to Cells and EVs

(A) Buffy coat cells were incubated with CPP-FAM, washed, and imaged using an Olympus BX62 microscope or quantified using a BD LSR II flow cytometer (BD Biosciences, NJ, USA). The respective histograms show autofluorescence (red) and penetration by CPP-FAM (blue).

(B) Dot-plot profile of RBCs.

(C) Penetration of RBC-membrane by CPP-FAM.

(D) Dot-plot profile of plasma EVs (arrow).

(E) Penetration of EV membrane by CPP-FAM (blue histogram). Incubation of EVs-CPP-FAM with 0.2% trypan blue does not decrease the fluorescence signal compared to buffer-treated sample (red histogram, behind the blue). Orange histogram represents the autofluorescence of EVs. Experiments performed four times.

isolated buffy coat cells with 20 mM CPP-FAM for 20 min at RT without mixing (Figures 2A–2C). Our results show that, although all the circulating cells tested were labeled by CPP-FAM, the intensity of the signal varied significantly with the cell type. Platelets, lymphocytes, and PMNs had the lowest signals (MFI 964, 1,800, and 3,645, respectively) and RBCs and monocytes the highest (MFI 9,803 and 18,710, respectively). The variation was likely due to differences in the cell volume, internal pH, and, possibly, membrane composition. For lymphocytes, a subpopulation of 14.1% had a higher CPP-FAM uptake than the remaining 85.9%. We next tested (Figures 2D and 2E) the penetrating capabilities of CPP-FAM on EVs by incubating cell-free plasma with a diluted solution of CPP-FAM for 20 min at RT, following our published protocols (Danielson et al., 2016; Shah et al., 2017) with 2 ng/mL CPP-FAM. After 20 min, the mixture was analyzed, without washing, by nano-flow cytometry. Our data show a unimodal shift of the EV fluorescence following CPP-FAM treatment (Figure 2E, blue histogram, versus plasma control, orange), strongly suggesting that CPP-cargo penetrates all plasma EVs, without bias for a certain membrane type or cell origin. An alternative explanation could be that a population of CPP-FAM became attached to the outer leaflet of all circulating EVs, as it is commonly seen in cells pretreated with CPP-FAM (Illien et al., 2016). We investigated this alternative explanation by using FAM as the fluorophore bright as it is quenchable by trypan blue treatment. Thus, we tested whether the FAM fluorescence was originating from within the EVs, was associated with the plasma membrane, or both by incubating an aliquot of the EVs-CPP-FAM mixture with 0.2% trypan blue for 5 min. Our results showed that the fluorescence intensity did not change measurably following trypan blue-mediated quenching (Figure 2E red histogram behind the blue), strongly indicating that CPP-FAM complexes were in fact inside the EVs and therefore not quenchable in the trypan blue. While the signal associated with CPP-FAM depends almost exclusively on the amount of probe trapped by each EV, and thus by the EV volume, the signal intensity for a specific miRNA-CPP-FAM depends on the number or RNA targets when detecting specific RNA molecules by molecular beacons could be significantly lower.

Detection of Cell-Specific EV miRNAs by CPP-MBs

We designed a CPP-miRNA-MB against miR-495, an miRNA enriched in circulating platelets and also relevant in the pathogenesis of a number of cancers (Chen et al., 2017a; Li et al., 2016). Our results in Figure 3A show that incubation of whole blood with CPP-miR495-MB for 5 min at RT resulted in specific and strong labeling of the platelet population without any detectable labeling of the red blood cells or nucleated cells, even after 30 min of imaging. The CPP-miR495-MB labeling of the platelets (arrows in Figure 3A1) was both diffusely distributed throughout the cytoplasm and compartmentalized in vesicle-like structures, possibly primary- or alpha-granules (inset in Figure 3A1, upper left panel). Other circulating cells present in the blood, such as RBCs, seen as concave shadows, and PMNs, outlined in Figure 3A2–4, did not display any detectable signal in the cytoplasm. However, overnight incubation of whole blood with MBs showed discreet punctuated fluorescent pattern in circulating neutrophils, possibly in the lysosomal compartment. We next tested the efficacy of CPP-MBs to label platelet-specific EVs by imaging cell-free plasma incubated with CPP-miR495-MB using double-immersion, high-resolution dark field imaging (Figure 3B) achieved by immersion of both the high-numerical aperture (NA) cardioid-type condenser (NA = 1.4) and the 100x1.35 PlanApo objective fitted with iris diaphragm, coupled to fluorescence microscopy (Figure 3C) or by nano-flow cytometry (Figure 3D and 3E). Although dark-field microscopy has the advantage of identifying smaller particles with sizes down to 20–40 nm (Craig et al., 2010), it cannot differentiate between EVs and other particles such as lipoprotein complexes and protein aggregates within the same size range. The lack of registration between the dark-field and the fluorescence signals (arrows in Figures 3B and 3C) was likely due to (1) the Brownian motion of certain EVs, (2) the short exposure time required for dark-field images, and (3) the relatively long exposure times (tens to hundreds of milliseconds) for the fluorescence acquisition. When using fluorescence microscopy, the percent positive populations for CPP-miR495-MBs varied between 3% and 8%, depending on the donor. Analyzing the same specimen by nano-flow cytometry using miR495-MB

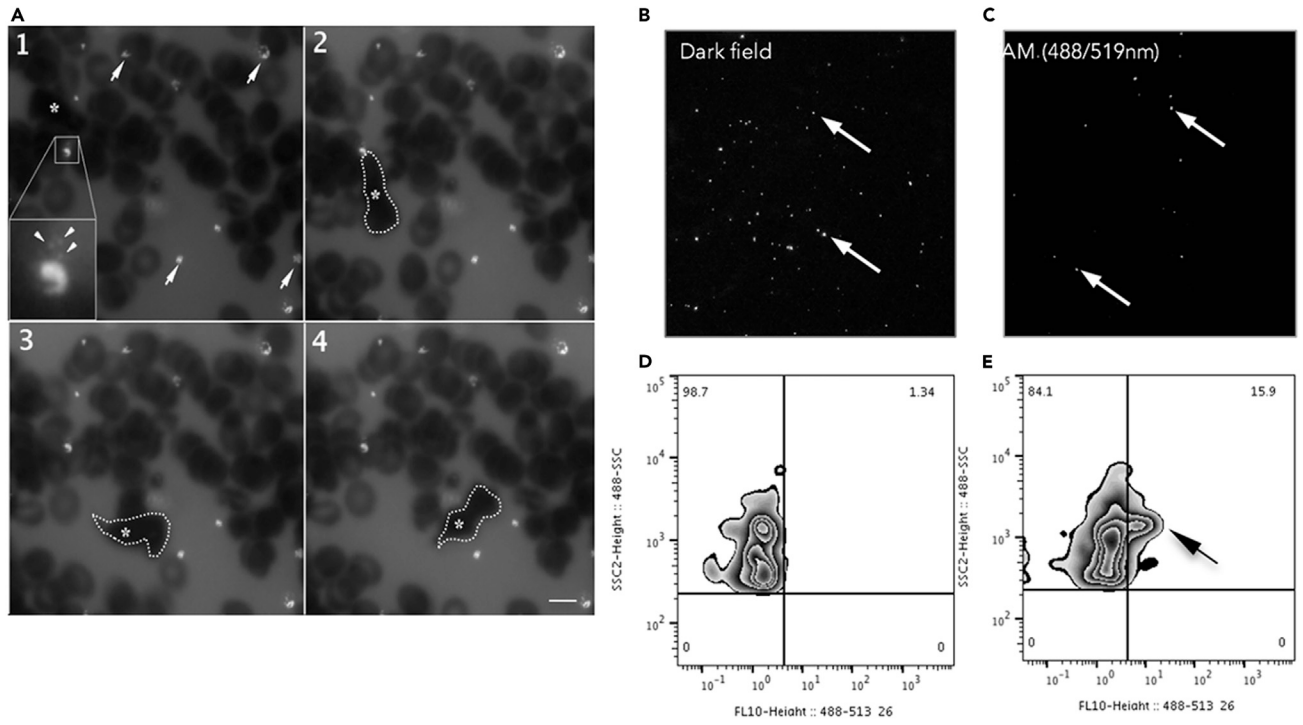

Figure 3. Detection of EV miR-495 by Molecular Beacons

(A) Detection of platelet-associated miR-495 by fluorescence microscopy (arrows).

(B–E) (B) Detection of EV by dark-field microscopy and (C) miR-495-**specific** signal by fluorescence microscopy (arrows). Nano-flow cytometric profile of plasma EVs probed with either MB-miR-495 (D) or MB-miR495 coupled to cell penetrating peptide (E). Experiments performed three times, with similar results.

without the cell penetrating peptide as negative control identified a CPP-miR495-MB-positive population between 13% and 18%, again depending on the donor (Figures 3D and 3E). One explanation for the lack of correlation between the two measurements could be attributed to the increased detection of EV and non-EV particles when using dark-field microscopy compared with nano-flow cytometry. Our results indicate that these combined methods allow an approximate characterization of the MB-generated signal and the percent of positive nanometer-sized structures.

The RBC miRNA451 Expression Levels Are Variable among Donors

Human RBCs contain several miRNA species, some of which were described to be relevant in malaria pathogenesis as well as certain inflammatory conditions (Babatunde et al., 2018; Mantel et al., 2013). We tested the ability of CPP-MB to detect the amount of miRNAs in human RBCs and RBC-derived EVs using fluorescence microscopy, flow cytometry, and dark-field microscopy. Incubation of RBCs with 2 μg of CPP-MB miR451a RBCs for 1 h at 37°C, followed by labeling of the RBCs with a membrane stain (CellMask green) generated a distinct punctuated pattern in RBCs cytoplasm with some RBCs showing significantly higher levels of RBC miR451a than others, likely due to differences in the circulatory age of RBCs, similar with the total RNA staining. Figure 4A also shows that the vast majority of the signal originated from under the plasma membrane, suggesting that the MB could not penetrate deeper into the RBC, lack of miRNAs in areas away from the plasma membrane, or an inhibitory effect of hemoglobin on the fluorochromes. We next used real-time super-resolution microscopy (SRRF), a method that uses a combination of temporal fluctuation analysis and localization microscopy. This is a relatively recent (2016) (Culley et al., 2018) super-resolution method, which unlike classical super-resolution imaging methods that require use of laser-based illumination, extended acquisition and processing times, involved samples preparation, and dedicated fluorochromes, allows acquisition of super-resolution imaging of standard fluorescence samples in seconds. Our results show the same RBC imaged either with standard fluorescence microscopy (FL) or SRRF (Figure 4, upper panel). SRRF clearly identifies discreet MB signals including a miR451a MB located inside the cytoplasm, as well as an EV-like structure (arrows in insert), suggesting that super-resolution

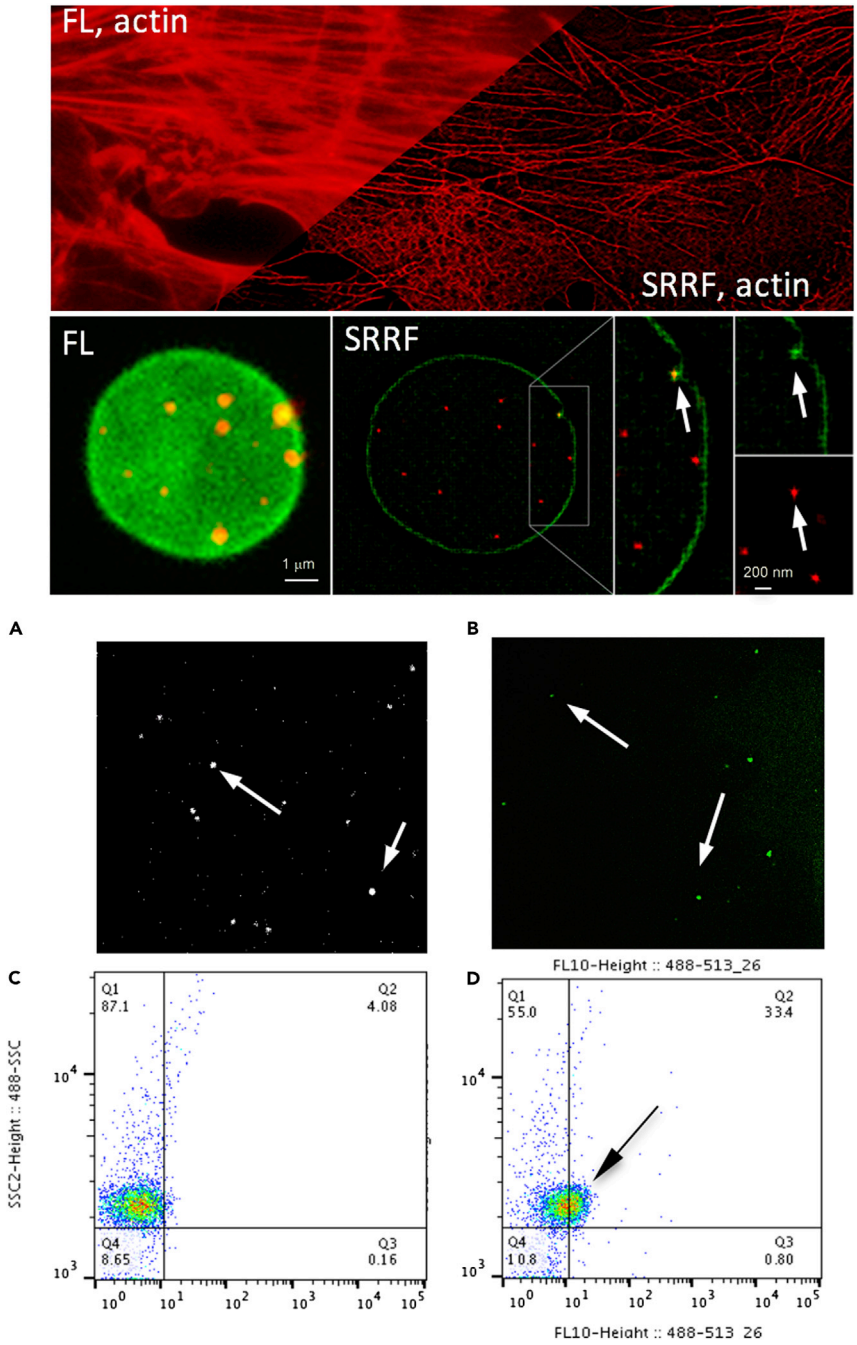

Figure 4. Imaging MB Staining with Super Resolution Microscopy, and Detection of EV miR451a by Molecular Beacon

Top. Increase spatial resolution of actin filaments when imaged by SRRF compared with standard fluorescence. Bottom. (A) RBC labeled with membrane dye (CellMask, green) and CPP-MB-miR451a-Alexa 594 (red) was imaged sequentially with standard fluorescence microscopy (FL, left) followed by SR microscopy (SRRF, right). Inset arrow shows MB signal originating from an EV-like membrane structure located near plasma membrane (arrows). Detection of total EVs by high-resolution dark-field microscopy (arrows).

(B) Detection of EV miR451a-specific signal by fluorescence microscopy (arrows).

(C and D) (C) Nano-flow profile of plasma EVs probed with either non-penetrating MB-miR451a (C) or membrane-penetrating CPP-MB-miR451a shows a 30% positive EVs (D). Experiments performed three times, with similar results.

microscopy permits better quantification and localization of signals originating from MBs than standard fluorescence microscopy. Somehow unexpectedly, co-staining of RBC RNA with Syto9, a pan-RNA probe, and CPP MB-miR451a showed limited, if any, co-localization between miRNA451 and the Syto-9 labeled small RNA, likely, t and rRNAs (data not shown). Similar to the results obtained when investigating platelet-derived EVs by dark-field microscopy, fluorescence, and nano-flow cytometry, interrogation of RBC-derived EVs (see Figure 4A and B) rendered similar results with approximately 30% of the total circulating EVs being positive for red-cell-specific miRNA-451 (Figure 4C and D).

Validation of MB-Based Signal by qRT-PCR

We next performed qPCR analysis of miR451a using increasing numbers of RBCs from five unique donors. Although the standard curve showed as expected, a linear increase in the miR signal with the number of cells used for RNA extraction (from 10^3 to 10^8R > 0.94), our results also indicate that the amount of miR451a/RBC was significantly different among donors. Our analyses (Figures 5A and 5B), which were performed three times over a period of 8 weeks, showed that certain individuals consistently expressed higher number of miR451a copies/RBC (average $\mathbf{C_t}$ 13/10^8RBCs), or fewer copies of miR451a (average C_t 22/10^8RBCs). However, in several donors, the levels of RBC miR451a changed significantly, possibly due to changes in the proportion of circulating, new RBCs, which contain higher amounts of RNA compared with the older RBCs (see Figure 1B). We also noted that the detection of the RBC RNA when using fewer than 10,000 RBCs becomes unreliable (Ct values above 35).

A similar high/low expression pattern was noted in the expression levels of miR451a in circulating RBCs when using MBs and flow cytometry, with certain healthy donors displaying higher levels of miR451a (MFI = 72), compared with low expressers, MFI of 44 on average (see Figures 5C and 5D). Next, we measured the expression levels of RBC miR451a by flow cytometry in seven healthy donors, by incubating CPP-MB-miR451a with *parent RBCs* or *complement-generated EVs*. Most complement-generated EVs contained detectable amounts of miR451a, and overall the levels of miR451a in EVs, as detected by CPP-MB miR451a, matched those of parent RBCs (Figure 5E). Specifically, high miR451a RBCs expressers ($MFI_{miR451a\ RBC}$ = 37.0) released EVs with high miR451a signal, $MFI_{miR451a\ EVs}$ = 113.4, whereas low miR451a RBCs expressers $MFI_{miR451a\ RBC}$ = 18.0, generated EVs with lower fluorescence signal $MFI_{miR451a\ EV}$ = 52.7. These findings would suggest that, at least in the case of RBCs and miR451a, the expression-level profile of the parent cells is mirrored in EVs. The fluorescence values generated by MBs in EVs were higher than those measured in parent RBCs probed with the same MBs, probably due to the inhibitory effect of hemoglobin on beacon fluorescence. The electron microscopy analysis of RBC-EVs show low to no detectable levels of hemoglobin in RBCs, which may explain the higher MB fluorescence of EVs compared with that of the parent cell.

We next contrasted the data obtained when using flow cytometry and CPP-MBs by comparing the flow cytometry results with the gold standard method for detecting miRNA gene expression levels, quantitative PCR. We collected blood from five self-declared healthy donors and measured the expression levels of miR451a in RBCs and RBC-EVs by qPCR. Our results showed no correlation (R = 0.16, data not shown) between the levels of miR451a isolated from RBCs and RBC-EVs collected from low, intermediate, and high miR451a expressers measured by quantitative PCR, even when accounting for the number of RBC-EVs used for RNA quantification, measured by time-gated nano-flow cytometry (Figures 5F and S3).

Taken together, our results suggest that, even if there is little agreement between the two EV miRNA quantification approaches, using the one-step MB-based detection method and flow cytometry could provide a rapid, qualitative process for EV RNA detection. This approach is currently limited by the detection of weak fluorescence in rapid flow conditions, although new instruments are being developed using significantly slower flow rate to address this very issue (Morales-Kastresana et al., 2019).

DISCUSSION

Characterizing EV RNA profiles is a difficult task owing to methodological impediments during the EV isolation and purification steps, which are further amplified by convoluted extraction protocols of already low quantities of RNAs present in EVs, as well as the involved biocomputational analyses of the RNA data. In addition, most EV isolation protocols rely on the assumption that the expression levels of the certain RNA targets present in tissue-specific EVs are abundant enough to stand out against the background noise generated by the RNA present in the rest of the EVs. Our data shown in Figure 1 indicate that, even from

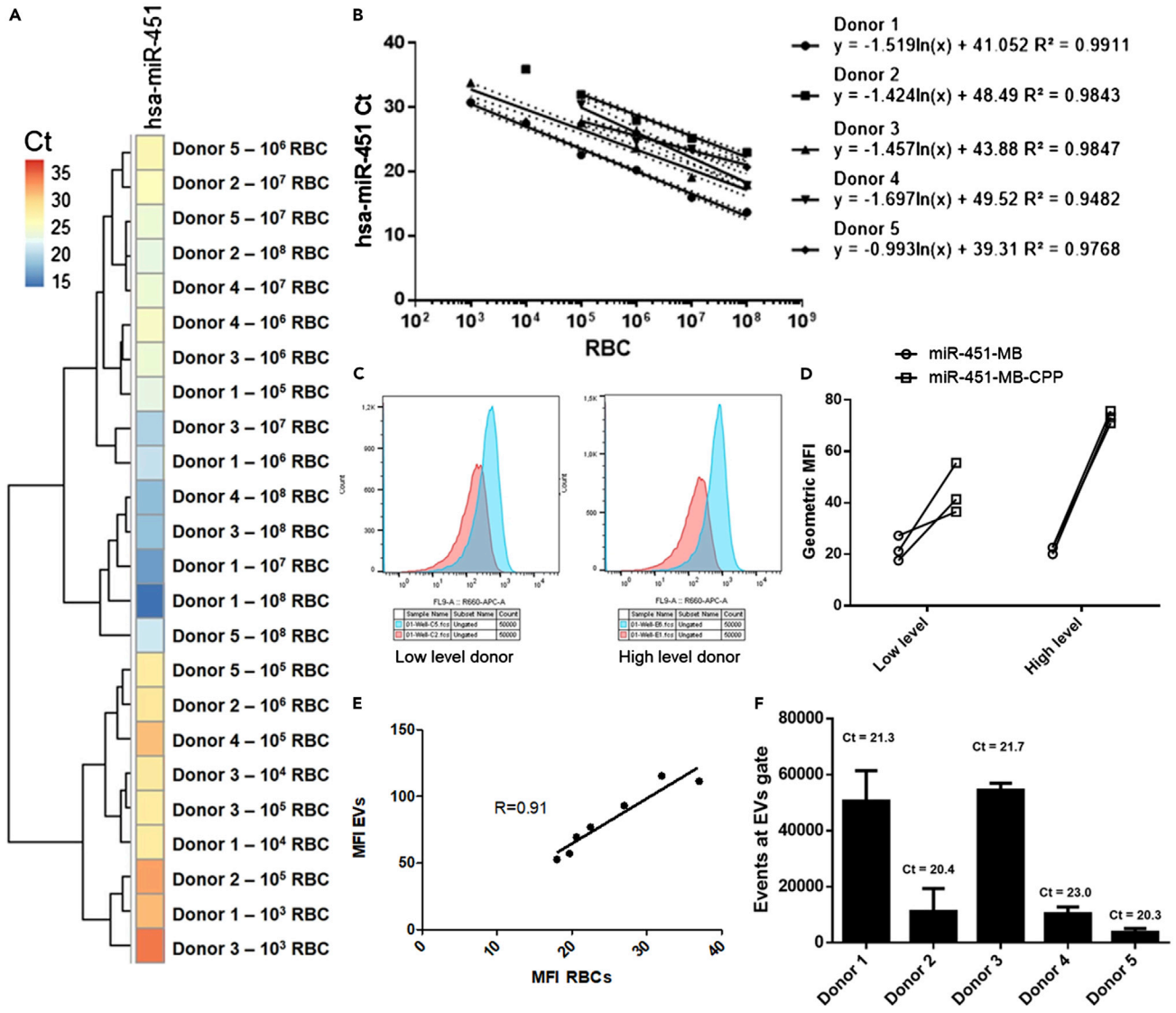

Figure 5. qPCR Corroborates Molecular Beacon-Based Flow Cytometric Data

RNA from 10^8 to 10^3 RBCs was extracted from five donors, and hsa-miR451a was analyzed by qPCR. Heatmap showing all Ct levels from all samples were clustered showing miRNA-451 levels from high- and low-expression donors (A). Standard curves were generated showing a linear relationship between miRNA Ct levels and the final amount of RBC (B). Flow cytometry data showed higher geometric MFI for higher-expression-level donor compared with low-expression donor (C and D). Nano-flow cytometry showed the correlation between miR451a from parent RBCs and complement-generated EVs (E). Nano-flow cytometry was used to estimate the concentration of RBC-derived EVs obtained from high and low miR-451a expression donors (F).

homogeneous cell types, such as RBCs, generation of EVs using complement activation produces EV populations heterogeneous in size and variable in RNA abundance. Therefore, enrichment protocols, even when using cell-type specific surface markers, may underappreciate or could even miss relevant RNA signals if their number is low.

Detection and quantification of EVs by flow cytometry has been made possible recently by the advent of new-generation instruments geared toward detection of small particles both by scatter and fluorescence signature. To date, detecting flow-based EV surface protein profiles relies either on direct antibody-based detection or on capturing the EV subsets by specific bead-bound antibodies targeting surface proteins. Extrapolating these methods to detection of specific RNA molecules is of little use owing to the shielding effect of the vesicle membranes.

Currently, there are several methods of introducing molecules into cells when interrogating the cargo with specific probes: (1) derivatizing the probes with acetoxymethyl (AM) groups; this approach, which in fact is a functional labeling, depends on the presence and activity of cytosolic esterases and is effective only for cargos below 0.6–0.8 kDa; (2) incorporating the probes into liposomes; although liposomes are the most effective delivery system, their fusion efficacy strictly depends on the physicochemical properties of their membranes, those of the target membranes, on their size, surface charge, and lipid organization (Bozzuto and Molinari, 2015). However, this approach was used successfully before as a means to detect RNA EV by fusing EVs with immobilized lipid nanospheres containing specific MBs; (3) cell/membrane-penetrating peptides (CPPs). We chose CPPs (based on HIV Tat peptide and PNABio-proprietary sequence), a more expensive alternative, but fast, highly effective, and, importantly, membrane-type agnostic, as seen in Figure 1.

MBs represent an attractive alternative for identification of specific RNA molecules owing to their specificity, ease of use, high signal to noise ratio, and the use of standard fluorochromes, which are easily detectable by instruments routinely used in virtually all research and clinical laboratories. Therefore, to overcome the current technological limitation of EV detection and RNA interrogation, we proposed herein an approach that combines the advantages of analyzing hundreds of thousands to millions of EVs, allowed by small particle flow cytometry, with the sensitivity and ease of use of RNA detection permitted by MBs. We next circumvented the inability of standard MBs to cross the EV membranes by attaching to MB membrane-penetrating peptides, an approach that was used for over 20 years to introduce small molecules in cells, but never with EVs. Recently, a fluorimeter-based detection method for MBs in EVs has been reported (Rhee and Jeong, 2017). The method uses Streptolysin O for permeabilization of EVs to allow MBs access to the RNA targets. We believe our approach, which does not rely on creating pores in plasma membrane, thus preventing the putative loss of molecules with MW under and of 100 kDa, may provide a more accurate representation of the miRNAs EV landscape. Figures 2 and 3 show that the method presented here can be readily used for the detection of specific RNA sequences by microscopy, as well as flow cytometers with nanometer resolution. The main disadvantage when using microscopy for EV detection is the Brownian motion, which may limit the detection of weak signals, or generate image artifacts. However, for immobilized EVs, either by using poly-L-lysine or capture antibodies-coated slides, microcopy offers significantly longer integration times (seconds) compared with flow cytometry (tens of microseconds) and is therefore better suited at detecting dim signals. Somehow unexpected, SR imaging the MB-based signal in cells did not reveal more structural details than regular high-resolution fluorescence microscopy, nor did it provide better quantification of the signal. It is possible that other super-resolution microscopy techniques with better resolving power may uncover yet unidentified details regarding the dynamics and behavior of individual miRNAs in cells and EVs.

If our results regarding the predetermined levels of miRNA451 in human circulating RBCs, obtained from a very limited number of self-declared healthy donors, can be validated in larger cohorts, it could have significant clinical implications. We have recently shown that miRNA451-rich EVs are released by circulating RBCs during malaria infection and fuse with and trigger a specific response in endothelial cells. Endothelial cell dysfunction in brain capillaries is a critical step leading to cerebral malaria, a complication with mortality of over 30%. Although signaling pathways involved several checkpoints and are redundant, these findings may suggest that the miR451a levels present in circulating RBCs could predispose patients with malaria to severe cerebral complication of malaria, and even death. A quick CPP-MB-based test readable by standard flow cytometry could help triage the patients at risk.

It is also worth noting that the number of cells in the subpopulation of lymphocytes having a larger uptake of CPP-FAM (14.1%) matches the ratio of B lymphocytes (5%–15%) in blood. This could suggest that B lymphocytes are more likely to be penetrated by CPP than T lymphocytes, although further studies would be needed to show whether this is the case or if this is just a coincidence.

There are several limitations in extrapolating the RNA detection results obtained by flow cytometry to those generated by qPCR, as we presented them in Figure 5. Although currently flow cytometry still lacks single EV sensitivity, it allows detection of fluorescence-associated signal for each trigger event, therefore permitting quantification of the MB-associated signal, which likely originates from several MBs and several EVs. On the other hand, qPRC has a sensitivity superior to that of flow cytometry-based RNA detection, but

it is vulnerable to slight variations in EV input. Our results in Figure S3 show that the same method of EV generation (complement activation), using the same number of RBCs (10^9), can generate vastly different numbers of EVs depending on the donor. In addition, the proportion of circulating new RBCs compared with old (Figures 1A and 1B) would likely generate EVs with different RNA cargo loads (Figure 1G) further underscoring the need for normalization of the results based on the number of EVs used for analysis.

In summary, we have described a rapid and precise detection method that (1) allows identification of EV subpopulations based on specific sequences of RNA that is (2) compatible with standard fluorescence microscopes and nano-flow cytometers, (3) can be used with other MBs or antibodies against protein targets, for multiplex-RNA/protein type analyses, and (4) can be used for sorting of EV subsets with specific RNA sequences for further downstream validation and discovery work.

Limitation of the Study

The ability of flow cytometers to identify and measure individual EVs is still controversial, and the signal read by the instrument and assigned to one trigger event may in fact represent an average of signals originating in many EVs of various fluorescence and size profiles. Similarly, the fluorescence of one MB may be too weak to be reliably detected by the flow cytometer detector in the limited time (in average 22 μs) afforded to signal acquisition during the passage of the EV in front of the interrogation area of the instrument. MB detection limit may be constrained by the low volume of the EV and the steric hindrance of the MB-target miRNAs creating a negative bias against the actual miRNAs abundance. These suggest that, unlike fluorometers, which can integrate the MB fluorescence signal over tens of seconds, current flow cytometers can only detect signals originating from MBs if the fluorescence is bright enough for the limited dwell time of the signal on the detector. An added complication when detecting specific sRNA fluorescence signal originating from EVs is their reduced size range and limited number of RNA copies per EV. Although MBs present a novel avenue for detecting miRNAs inside EVs when paired with CPPs, this method is still subject to the inherent difficulties common to all MB experiments. Fluorescent intermittency, or blinking (Lukinavicius and Johnsson, 2014), common in all nanoscale light sources, depends on the power of light source, the length of exposure, and power-law distribution of the "on" and "off" fluorescence over time. Systems that have a power-law distribution do not have a characteristic scale, meaning that the state of the MB cannot be accurately predicted at a given time point. This implies that it is unlikely that repeated flow cytometric measurements under the same conditions would yield the same fluorescence intensity over time.

METHODS

All methods can be found in the accompanying Transparent Methods supplemental file.

SUPPLEMENTAL INFORMATION

Supplemental Information can be found online at https://doi.org/10.1016/j.isci.2019.100782.

ACKNOWLEDGMENTS

This publication is part of the United States National Institute of Health (NIH) extracellular RNA communication consortium paper package and was supported by the NIH Common fund's exRNA Communication Program.

This work was supported by the following grants to I.C.G. from the NIH: HL126497, HL147353, CA218500, UG3TR002881.

AUTHOR CONTRIBUTIONS

G.P.O.J., I.C.G., J.J., T.J.-T., and S.T. designed the experiments and discussed about experimental results. G.P.O.J., E.Z., G.R., D.D., and S.L. performed the experiments pertinent to imaging and testing the molecular beacons. E.Z., G.R., and J.T. performed the nano-flow analyses, instrument settings, and result analyses. G.P.O.J., I.C.G., and E.Z. wrote the manuscript. T.J.-T. and S.T. provided detailed comments regarding the manuscript.

DECLARATION OF INTERESTS

The authors declare no competing interests.

Received: March 6, 2019
Revised: December 2, 2019
Accepted: December 12, 2019
Published: January 24, 2020

REFERENCES

Rhee, W.J., and Jeong, S. (2017). Extracellular vesicle miRNA detection using molecular beacons. Methods Mol. Biol. *1660*, 287–294.

Shah, R., Yeri, A.S., Das, A., Courtright-Lim, A., Ziegler, O., Gervino, E., Ocel, J., Quintero Pinzon, P., Wooster, L., Shields Bailey, C., et al. (2017). Small RNA-seq during acute maximal exercise reveal RNAs involved in vascular inflammation and cardiometabolic health. Am. J. Physiol. Heart Circ. Physiol. *313*, H1162–H1167.

Thery, C. (2015). Cancer: diagnosis by extracellular vesicles. Nature *523*, 161–162.

Tkach, M., and Thery, C. (2016). Communication by extracellular vesicles: where we are and where we need to go. Cell *164*, 1226–1232.

Tyagi, S., Bratu, D.P., and Kramer, F.R. (1998). Multicolor molecular beacons for allele discrimination. Nat. Biotechnol. *16*, 49–53.

Tyagi, S., and Kramer, F.R. (1996). Molecular beacons: probes that fluoresce upon hybridization. Nat. Biotechnol. *14*, 303–308.

Vargas, D.Y., Raj, A., Marras, S.A., Kramer, F.R., and Tyagi, S. (2005). Mechanism of mRNA transport in the nucleus. Proc. Natl. Acad. Sci. U S A *102*, 17008–17013.

Vives, E., Richard, J.P., Rispal, C., and Lebleu, B. (2003). TAT peptide internalization: seeking the mechanism of entry. Curr. Protein Pept. Sci. *4*, 125–132.

Walzer, K.A., and Chi, J.T. (2017). Trans-kingdom small RNA transfer during host-pathogen interactions: the case of *P. falciparum* and erythrocytes. RNA Biol. *14*, 442–449.

Babatunde, K.A., Mbagwu, S., Hernandez-Castaneda, M.A., Adapa, S.R., Walch, M., Filgueira, L., Falquet, L., Jiang, R.H.Y., Ghiran, I., and Mantel, P.Y. (2018). Malaria infected red blood cells release small regulatory RNAs through extracellular vesicles. Sci. Rep. *8*, 884.

Bonnet, G., Tyagi, S., Libchaber, A., and Kramer, F.R. (1999). Thermodynamic basis of the enhanced specificity of structured DNA probes. Proc. Natl. Acad. Sci. U S A *96*, 6171–6176.

Bozzuto, G., and Molinari, A. (2015). Liposomes as nanomedical devices. Int. J. Nanomed. *10*, 975–999.

Bratu, D.P., Cha, B.J., Mhlanga, M.M., Kramer, F.R., and Tyagi, S. (2003). Visualizing the distribution and transport of mRNAs in living cells. Proc. Natl. Acad. Sci. U S A *100*, 13308–13313.

Chen, H., Wang, X., Bai, J., and He, A. (2017a). Expression, regulation and function of miR-495 in healthy and tumor tissues. Oncol. Lett. *13*, 2021–2026.

Chen, M., Ma, Z., Wu, X., Mao, S., Yang, Y., Tan, J., Krueger, C.J., and Chen, A.K. (2017b). A molecular beacon-based approach for live-cell imaging of RNA transcripts with minimal target engineering at the single-molecule level. Sci. Rep. *7*, 1550.

Craig, G.A., Allen, P.J., and Mason, M.D. (2010). Synthesis, characterization, and functionalization of gold nanoparticles for cancer imaging. Methods Mol. Biol. *624*, 177–193.

Culley, S., Tosheva, K.L., Matos Pereira, P., and Henriques, R. (2018). SRRF: universal live-cell super-resolution microscopy. Int. J. Biochem. Cell Biol. *101*, 74–79.

Danielson, K.M., Estanislau, J., Tigges, J., Toxavidis, V., Camacho, V., Felton, E.J., Khoory, J., Kreimer, S., Ivanov, A.R., Mantel, P.Y., et al. (2016). Diurnal variations of circulating extracellular vesicles measured by nano flow cytometry. PLoS One *11*, e0144678.

Giesendorf, B.A., Vet, J.A., Tyagi, S., Mensink, E.J., Trijbels, F.J., and Blom, H.J. (1998). Molecular beacons: a new approach for semiautomated mutation analysis. Clin. Chem. *44*, 482–486.

Illien, F., Rodriguez, N., Amoura, M., Joliot, A., Pallerla, M., Cribier, S., Burlina, F., and Sagan, S. (2016). Quantitative fluorescence spectroscopy and flow cytometry analyses of cell-penetrating peptides internalization pathways: optimization, pitfalls, comparison with mass spectrometry quantification. Sci. Rep. *6*, 36938.

Kreimer, S., Belov, A.M., Ghiran, I., Murthy, S.K., Frank, D.A., and Ivanov, A.R. (2015). Mass-spectrometry-based molecular characterization of extracellular vesicles: lipidomics and proteomics. J. Proteome Res. *14*, 2367–2384.

Kuo, W.P., Tigges, J.C., Toxavidis, V., and Ghiran, I. (2017). Red blood cells: a source of extracellular vesicles. Methods Mol. Biol. *1660*, 15–22.

LaMonte, G., Philip, N., Reardon, J., Lacsina, J.R., Majoros, W., Chapman, L., Thornburg, C.D., Telen, M.J., Ohler, U., Nicchitta, C.V., et al. (2012). Translocation of sickle cell erythrocyte microRNAs into *Plasmodium falciparum* inhibits parasite translation and contributes to malaria resistance. Cell Host Microbe *12*, 187–199.

Li, J.Z., Wang, Z.L., Xu, W.H., Li, Q., Gao, L., and Wang, Z.M. (2016). MicroRNA-495 regulates migration and invasion in prostate cancer cells via targeting Akt and mTOR signaling. Cancer Invest. *34*, 181–188.

Lukinavicius, G., and Johnsson, K. (2014). Fluorescence microscopy: strategic blinking. Nat. Chem. *6*, 663–664.

Mantel, P.Y., Hoang, A.N., Goldowitz, I., Potashnikova, D., Hamza, B., Vorobjev, I., Ghiran, I., Toner, M., Irimia, D., Ivanov, A.R., et al. (2013). Malaria-infected erythrocyte-derived microvesicles mediate cellular communication within the parasite population and with the host immune system. Cell Host Microbe *13*, 521–534.

Mantel, P.Y., Hjelmqvist, D., Walch, M., Kharoubi-Hess, S., Nilsson, S., Ravel, D., Ribeiro, M., Gruring, C., Ma, S., Padmanabhan, P., et al. (2016). Infected erythrocyte-derived extracellular vesicles alter vascular function via regulatory Ago2-miRNA complexes in malaria. Nat. Commun. *7*, 12727.

Marras, S.A., Kramer, F.R., and Tyagi, S. (1999). Multiplex detection of single-nucleotide variations using molecular beacons. Genet. Anal. *14*, 151–156.

Mhlanga, M.M., and Tyagi, S. (2006). Using tRNA-linked molecular beacons to image cytoplasmic mRNAs in live cells. Nat. Protoc. *1*, 1392–1398.

Morales-Kastresana, A., Musich, T.A., Welsh, J.A., Telford, W., Demberg, T., Wood, J.C.S., Bigos, M., Ross, C.D., Kachynski, A., Dean, A., et al. (2019). High-fidelity detection and sorting of nanoscale vesicles in viral disease and cancer. J. Extracell. Vesicles *8*, 1597603.

Nitin, N., Santangelo, P.J., Kim, G., Nie, S., and Bao, G. (2004). Peptide-linked molecular beacons for efficient delivery and rapid mRNA detection in living cells. Nucleic Acids Res. *32*, e58.

iScience, Volume *23*

Supplemental Information

Detection of Extracellular Vesicle RNA Using Molecular Beacons

Getulio Pereira de Oliveira Jr., Eric Zigon, Gaenna Rogers, Danny Davodian, Shulin Lu, Tijana Jovanovic-Talisman, Jennifer Jones, John Tigges, Sanjay Tyagi, and Ionita Calin Ghiran

Transparent Methods

Reagents;

Antibodies (Abs) were obtained as follows: nonimmune IgG1, (BD Biosciences, San Jose, CA); secondary antibodies: AlexaFluor-488 goat anti–mouse IgG, AlexaFluor-594 goat anti–rabbit IgG, and AlexaFluor-594 goat anti–mouse IgG (Thermo Fisher Scientific, Waltham, MA); Buffers and reagents: PBS, HBSS, $HBSS^{++}$, Trypan Blue, Syto9, Cell Mask (Thermo Fisher Scientific, Waltham, MA). Complement proteins**:** Human C5b,6 complex, Human C7 protein, Human C8 protein, Human C9 protein (Complement Technology, Inc. Tyler, TX)

Preparation of RBCs and buffy coat cells

The current study was approved by the Beth Israel Deaconess Medical Center Institutional Review Board (IRB). Two mL of fresh whole blood was obtained via venipuncture using Vacutainer EDTA tubes (BD, Franklin Lakes , NJ) from self-declared healthy volunteers. Hemoglobin concentration values for each donor were obtained using a hemoglobinometer (Hb 201+, HemoCue, Ängelholm, Sweden). White cells separated by passing the blood through an Acrodisc WBC syringe filter (Pall Corporation, NY, NY), washed twice at room temperature, centrifuged twice at 500xg. RBCs were re-suspended in HBSS with calcium and magnesium ($HBSS^{++}$), counted using a slide hemocytometer, and adjusted to concentrations specific for each experiment. For testing the CPP-FAM (**Fig. 2**), buffy coat cells were isolated by allowing venipuncture blood to settled at room temperature for 45 minutes, followed by two washes in HBSS $^{++}$. Cells were then incubated with CPP-FAM for 20 mins and analyzed by flow cytometry.

Separation of new and old RBCs

Two $x10^9$cells in 1.5 mL of HBSS $^{++}$ were loaded on top of 40 mL of self-forming Percoll gradient solution (30.76 mL Percoll (density 1.130 g/mL, GE Healthcare Bio-Sciences, Uppsala, Sweden), 4 mL 1.5 M NaCl, and 5.24 mL of deionized water) in a 30 mL centrifuge tube. The

tubes were centrifuged at 27,000 × g for 20 minutes. At the end of the centrifugation time, multiple layers of RBCs of different densities are formed within the tube, with the least dense (newest) in the top layer and the most dense (oldest) in the bottom layer. RBCs from the top and bottom layers were collected separately, washed twice in $HBSS^{++}$, resuspended at a concentration of 5×10^8 cells/mL, and RNA extracted and quantified as detailed below.

Generation of RBC-EVs by complement activation

RBCs, ($2x10^9$cells in 1.5 mL of $HBSS^{++}$) were incubate C5b-6 at a final concentration of 0.18μg/ml, on a shaker set at minimum, at 37°C. After 15 minutes, C7 was added to the cell suspension to a final concentration of 0.2μg/ml, and left on the shaker for and additional 5 minutes. C8 and C9 were then to a final concentration of 0.2μg/ml, and 0.45μg/ml respectively, and complement activation allow to continue for an additional 20 minutes. At the end of the incubation time, cells were centrifuged twice at 2.500×g for 10 minutes, and then 12,000xg for another 10 mins. The supernatant was loaded on a qEV column (Izon), and fractions 1-4 were collected using the AFC (Automatic Fraction Collector, iZon) and pooled into a volume of 2 milliliters. The resulting EV-containing volume was then concentrated using 10kDa cut-off Amicon Ultra-4 filter (Millipore, Burlington, MA) by centrifugation at 4,000xg for 10 minutes. Two hundred microliters of the final 400 uL final volume were then processed for EV RNA extraction as detailed below.

Synthesis of MB, CPP-MBs

All MBs were labeled with a fluorophore reporter dye (FAM, AlexaFluor 488, or AlexaFluor 647) at the 5′-end and a BHQ quencher at the 3′-end. All MBs were synthesized by either BioSynthesis (Lewisville, TX), or PNABio (Newbury Park, CA) with specific sequences as follows:

MiR-495: 5′-CGCGATCGAAGTGCACCATGTTTGTGATCGCG/BHQ-1//iSp18/-3’-Linker-CPP(*tat peptide*)-N-terminal of peptide

hsa-miR-30d-5p: 5'- rUrGrU rArArA rCrArU rCrCrC rCrGrA rCrUrG rGrArA rG -3'

hsa-mir-495-3p: 5'- rArArA rCrArA rUrGrG rUrGrc rArCrU rUrCrU rU -3'

hsa-miR-30d-5p: /56-FAM/CGCGATCCTTCCAGTCGGGGATGTTTACAGATCGCG/ZEN//iSp18//3Bio/

mir-495: /56-FAM/CGCGATCGAAGTGCACCATGTTTGTGATCGCG/ZEN//iSp18//3Bio/

hsa-miR451a: 5’A594-E-CTCAGTAATGGTAACG-CVSRRRRRRGGRRRR-Lys(BHQ1)3’

hsa-miR451a: 5’A594-E-CTCAGTAATGGTAACG- Lys(BHQ1)3’

Delivery of MB to EVs

Delivery of MB into the cells or EVs was assured by the presence of CPPs, either the TAT peptide or a low molecular-weight protamine peptide (LMWP). As controls, the same MBs were used without the attached CPPs of choice.

Coupling MBs to beads. Biotin-coupled MBs were attached to 6.57 um avidin beads following the manufacturer's instructions. Briefly, avidin-coated polystyrene particles (Spherotech, Inc., Cat. No. VP-60-5) were washed twice in PBS and coupled with 0.01mM miRNA MB (mir-30d or mir-495 biotinylated MB, IDT) already suspended in RNAse-free water in 0.1M PBS and left to incubate at room temperature for 1 hour. The beads where then centrifuged and washed in 1mL 0.1M PBS thrice at 20,000xg, resuspended in 405µL 1X PBS, and kept on ice until further use.

Dark field microscopy

For imaging EVs by dark field microscopy, the standard universal condenser was replaced with a double-immersion high NA (1.4) dark field cardioid condenser (Olympus Corporation, Walpole,

MA). The imaging was performed by double immersion, where both the condenser top lens and the 100X1.35 UPlanApo iris diaphragm objective were immersed in immersion oil. The iris diaphragm of the objective was closed such that the NA of the objective dropped just below that of the condenser, thus generating the dark field. Only slides with optimal thickness (1.1 mm) were used for imaging the EVs. This was ensured by imaging the focus spot formed on the frosted side of the slide when the cardioid condenser was moved to the max top position. If the image showed a dark (out of focus) disk surrounded by bright ring, instead of just a bright spot, the slide was considered unsuitable for optimal dark field imaging.

Preparation of Plasma and Isolation of EVs

Preparation of EVs was performed as described previously. (Danielson et al., 2016) Blood (5 mL) was obtained either by fingerprick or by percutaneous cubital venipuncture drawn in EDTA containing vacutainer (BD Biosciences, Franklin Lakes, NJ). Blood was centrifuged at 500 x *g* for 5 min to obtain plasma, followed by two centrifugations of 5,000 x *g* for 15 min and 12,000 x g for 15 minutes, respectively. Samples were processed in microcentrifuge tubes that showed no significant 'shed' plastic debris observed in the size range of EVs (USA Scientific, 1415-2500). The topmost lipid rich layer (1000-1500 µL) was discarded and 10 µL of the plasma was diluted to a final dilution of 1:1500 in Phosphate Buffered Saline (PBS; Life Technologies, Carlsbad, CA). All samples were analyzed by nanoFACS within 30 minutes post processing, and all procedures were performed at room temperature.

Electron Microscopy

RBCs were lightly fixed with 2.5% glutaraldehyde/2% formaldehyde in 0.1 M cacodylate buffer, pH 7.4, pelleted, resuspended in 2% low melting temperature sea plaque agarose (Sea Kem LE, Cambrex Bio Science, Rockland ME), cooled on ice to form a hard block of cells, and then fixed overnight at 4 degrees C in the same fixative. The agar block was post-fixed with 2%

osmium tetroxide, en bloc stained with 2% uranyl acetate, infiltrated with graded alcohols followed by propylene oxide, and embedded in LX112 resin. The resulting resin blocks of suspended cells were sectioned on an UltraCut E Ultramicrotome (Leica Microsystems, Inc., Buffalo Grove, IL) and placed on formvar and carbon-coated slot grids. Sections were stained with 2% uranyl acetate and lead citrate and then photographed using a JEOL 1400 electron microscope outfitted with an Orius SC1000 CCD camera (Gatan, Inc. Pleasanton, CA).

Nano Flow cytometry

The MoFlo Astrios EQ was set up according to the specifications detailed in "Characterization of EVs by Flow Cytometry" by Camacho et al. Briefly, quality control was performed according to the manufacturer's specifications using the automated QC and Calibration Beads (Beckman P/N B27034). After instrument adjustments have been performed, ApogeeMix (Cat #1493) is acquired to create a bead sizing curve and is used as a reference for further alignment adjustments with the micrometers to ensure maximum signal/noise ratio and dynamic range. Apogee beads are used because they range from 110nm to 1300nm consisting of unlabeled beads and fluorescently (525nm) labeled beads for added data assurance. The FSC voltage, SSC voltage, and threshold are adjusted to maximize the ApogeeMix signals and these settings remain constant during the acquisition of EVs. A raw data file was generated to determine instrument noise without sample contribution. In addition, $HBSS^{++}$ was used to dilute the plasma EVs to determine the existence of any additional background. Noise (which is the electronic noise attributed the instrument and is termed Dark Noise), events contributed by the background of $HBSS^{++}$ used for dilution of samples, and samples are gated accordingly and gates remain constant throughout the experiment. Dark noise is tracked to ensure instrument consistency and acts as an internal control. The stop criterion was set for time at 120s. Samples are acquired at a rate less than or equal to 10,000 events per second.

Extracellular Vesicle Sizing by qNano

The nanopores (CPC200, Izon) were stretched to 42-50mm, coated with 10% coating solution for 10 minutes, and then rinsed with 2% coating solution for 2 minutes. CPC 200 beads (1:500 dilution) with 2% coating solution were used to calibrate the machine and used as a reference in terms of both sizing and counting. Next, EVs (1:10 dilution) with 2% coating solution were analyzed following the manufacture's instructions. Prior to each run and between, the pores were washed twice with PBS. Samples were acquired at a voltage of 0.30V. The current was kept below 90-100nA with a noise ≈ 10nA. The applied pressure and vacuum were set at 0 and adjusted as necessary, but always kept the same throughout each experiment. When the current was stable, we started the data acquisition with 500 events or 10 mins acquisition time as end point.

RNA extraction, cDNA synthesis and qPCR from RBCs

RNA was extracted from isolated and purified RBCs collected from 5 self-declared healthy donors using MagMax mirvana total RNA isolation kit (Thermo Fisher, US), following manufacturer's instructions. For each donor, the number of RBCs used for RNA extraction increased by a factor of 10, from 10^3 to 10^8. RBCs were counted using a hemocytometer. Complementary DNA (cDNA) synthesis was performed using TaqMan Advanced miRNA cDNA Synthesis Kit (Thermo Fisher, US), and qPCR was performed in triplicate using Hsa-miR451a (001105 TaqMan assay ID) and TaqMan Fast Advanced Master Mix (Thermo Fisher, US) in 40 cycles of run in a 7500 Fast Real-time PCR System (Applied Biosystems, US.. Semi-log standard curves were generated by Graphpad prism, and the heatmap using Pheatmap package in R.

Supplemental Information

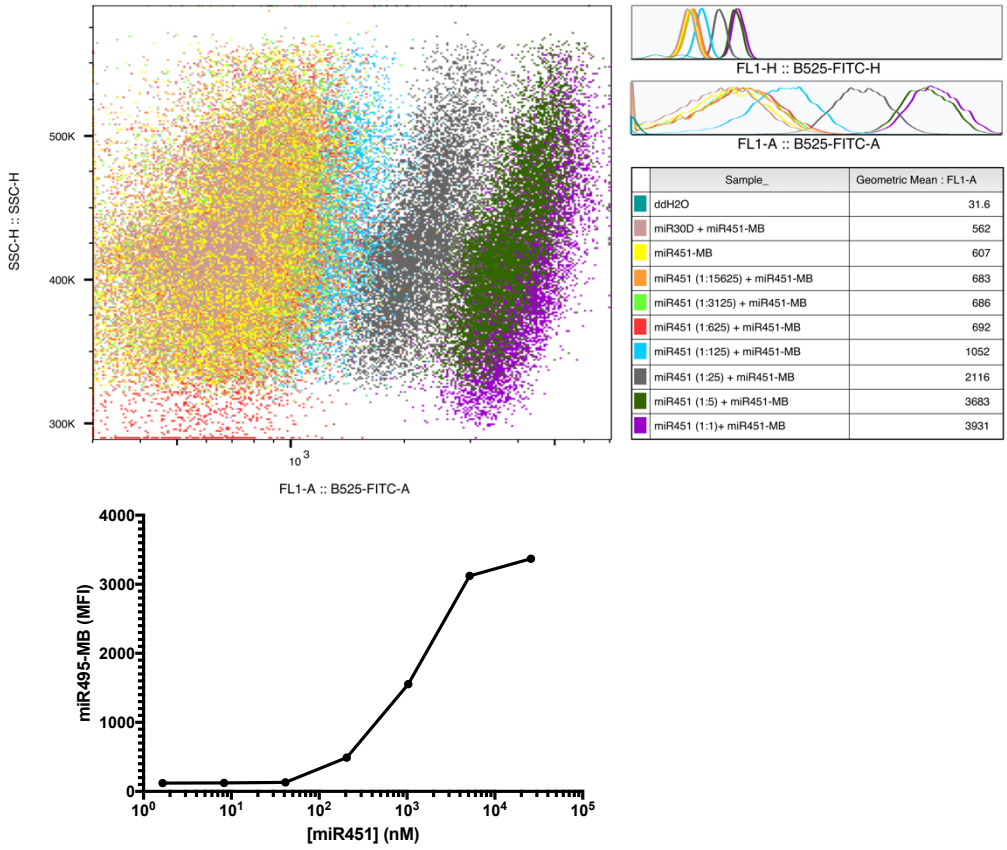

Figure S1. Flow cytometry of miRNA and bead-coupled miRNA-MBs, related to figure 2. A 5 fold serial dilution of miR451a (stock: 0.1mM) was made and 40 µL of the sample, 25µL streptavidin-sepharose (FITC) bead-coupled biotinylated miR451a-MB suspension, and 115µL RNAse-free water were sampled on a CytoFlex LX. miR30d was used as the unstained control. B525 –FITC channel was used for tracking the fluorescence intensity. 6 seconds of back flushing was performed between samples. Gains were set with the FSC at 25, SSC at 10, and the FITC channel at 50 with the automatic threshold based on the FSC. Sample flow rate was at 10µL/min. Abort rate was kept under 0.30% with about 240 events per second average. 10,000 events were recorded for analysis with stop criterion set at 10,000 events or 600 seconds. Geometric FITC mean were obtained from the FlowJo analysis software which is calculated from the intensity of the sample exceeds the mean of the unstained control. A clear positive correlation between the mean fluorescence intensity of beads carrying the molecular beacon with the histogram and dot plot overlay can be observed.

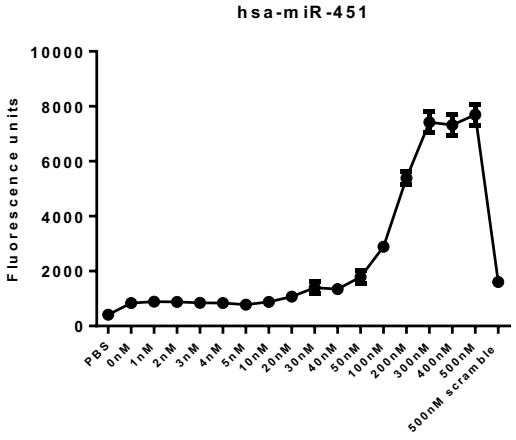

Figure S2. Specificity of molecular beacon coupled CPP for *in vitro* miR451a detection, related to figure 2. Increasing concentrations of targets were used and fluorescence was measured using a fluorescence plate reader.

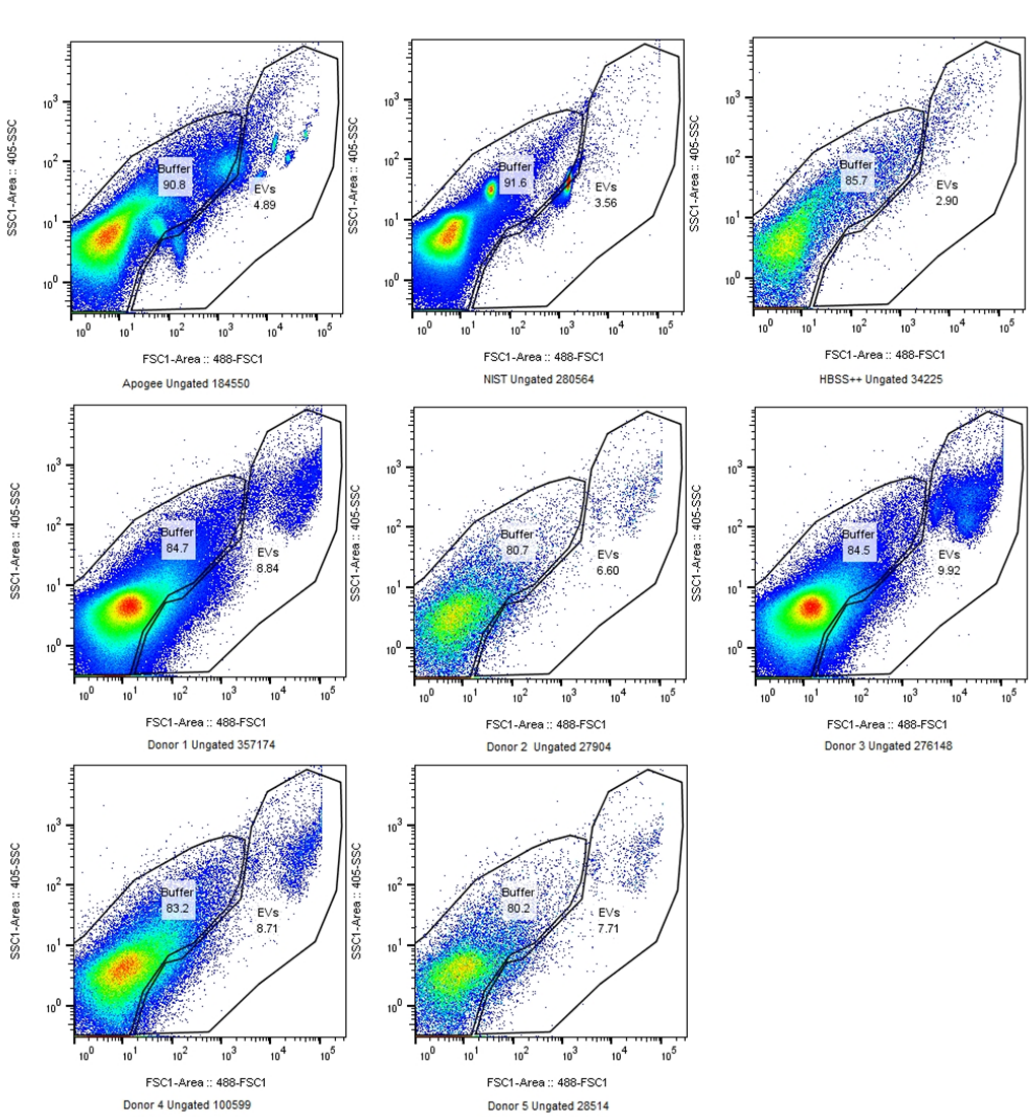

Figure S3. Detection of RBC-EVs by nanoFlow cytometry, related to figure 5. RBCs isolated and purified from 5 donors were treated with complement as discussed in Methods section, and EVs were purified by size exclusion chromatography. Apogee, NIST and HBSS^{++} buffer were used as a standard for gating and sizing purposes, and background noise respectively, (top row). Supernatants from buffer-, and complement-treated RBCs were recorded for 4 minutes, and event numbers in the EV gate recorded for normalization purposes.